Molecular Therapy
Nucleic Acids
Original Article

In Vivo RNAi-Mediated eIF3m Knockdown Affects Ribosome Biogenesis and Transcription but Has Limited Impact on mRNA-Specific Translation

Elena M. Smekalova,[1] Maxim V. Gerashchenko,[2] Patrick B.F. O'Connor,[3] Charles A. Whittaker,[1] Kevin J. Kauffman,[1] Anna S. Fefilova,[4] Timofei S. Zatsepin,[4,9] Roman L. Bogorad,[1] Pavel V. Baranov,[3,5] Robert Langer,[1,6,7,8] Vadim N. Gladyshev,[2] Daniel G. Anderson,[1,6,7,8] and Victor Koteliansky[4]

[1]David H. Koch Institute for Integrative Cancer Research, Massachusetts Institute of Technology, Cambridge, MA 02142, USA; [2]Division of Genetics, Department of Medicine, Brigham and Women's Hospital and Harvard Medical School, Boston, MA 02115, USA; [3]School of Biochemistry and Cell Biology, University College Cork, Cork T12 YN60, Ireland; [4]Skolkovo Institute of Science and Technology, Skolkovo, Moscow, 121205, Russia; [5]Shemyakin and Ovchinnikov Institute of Bioorganic Chemistry, RAS, Moscow 117997, Russia; [6]Department of Chemical Engineering, Massachusetts Institute of Technology, Cambridge, MA, USA; [7]Harvard-MIT Division of Health Sciences and Technology, Cambridge, MA, USA; [8]Institute of Medical Engineering and Science, Massachusetts Institute of Technology, Cambridge, MA, USA; [9]Department of Chemistry and Belozersky Institute of Physico-Chemical Biology, Lomonosov Moscow State University, Moscow 119234, Russia

Translation is an essential biological process, and dysregulation is associated with a range of diseases including ribosomopathies, diabetes, and cancer. Here, we examine translation dysregulation *in vivo* using RNAi to knock down the m-subunit of the translation initiation factor eIF3 in the mouse liver. Transcriptome sequencing, ribosome profiling, whole proteome, and phosphoproteome analyses show that eIF3m deficiency leads to the transcriptional response and changes in cellular translation that yield few detectable differences in the translation of particular mRNAs. The transcriptional response fell into two main categories: ribosome biogenesis (increased transcription of ribosomal proteins) and cell metabolism (alterations in lipid, amino acid, nucleic acid, and drug metabolism). Analysis of ribosome biogenesis reveals inhibition of rRNA processing, highlighting decoupling of rRNA synthesis and ribosomal protein gene transcription in response to eIF3m knockdown. Interestingly, a similar reduction in eIF3m protein levels is associated with induction of the mTOR pathway *in vitro* but not *in vivo*. Overall, this work highlights the utility of a RNAi-based *in vivo* approach for studying the regulation of mammalian translation *in vivo*.

INTRODUCTION

Translational control plays a role in a number of cellular homeostasis mechanisms, and alterations in translation can induce pathological conditions in humans. For example, genetic ribosomopathies, such as Diamond-Blackfan anemia and Schwachman-Diamond syndrome, are caused by the decreased expression of ribosomal proteins and translation factors.[1] An increase in the rate of protein synthesis makes cells prone to cancer.[2–4] The regulation of ribosome activity and number is a mechanism by which cells can adapt to stress.[5] Ribosome assembly accompanies diurnal cyclic changes in animal activity in quiescent hepatocytes in the liver.[6]

Modulation of the levels and/or activity of translation factors provides mechanisms for the reprogramming of gene expression and, thus, has a significant impact on cellular function.[7,8] For example, eukaryotic translation initiation factor eIF2 catalyzes tRNA binding to the small subunit of the ribosome, while modulation of eIF2 activity can induce changes in the translation of particular mRNAs that mediate response to stress, memory formation, and cancer development.[9] Translation initiation factor eIF4E recruits a small ribosomal subunit to mRNA; eIF4E overexpression can promote carcinogenesis by activating cancer-related signaling pathways.[10] Translation initiation factor eIF6 facilitates the association of small and large ribosomal subunits; variation in its expression modulates insulin sensitivity via specialized translation of lipogenic and glycolytic enzymes.[11] Translation initiation factor eIF3 stimulates several steps of translation initiation, including the binding of mRNA to the ribosome; recruitment of translation initiation factors eIF1, eIF1A, and eIF3; formation of the eIF2-Met-tRNAi^{Met}-GTP ternary complex; and ribosome recycling.[8,9] The downregulation of eIF3 subunits led to increased longevity in *C. elegans* (eIF3k and eIF3l subunits),[12] developmental disorders in zebrafish (eIF3h subunit),[13] and reduced malignant properties of the cells (eIF3a, -m, and -h subunits).[4]

The necessity to work with essential genes is one challenge in the study of the regulation of translation *in vivo*. Despite advances in engineering genetically modified mice, it remains challenging and

Received 3 June 2019; accepted 5 November 2019;
https://doi.org/10.1016/j.omtn.2019.11.009.

Correspondence: Daniel G. Anderson, David H. Koch Institute for Integrative Cancer Research, Massachusetts Institute of Technology, Cambridge, MA 02142, USA.
E-mail: dgander@mit.edu
Correspondence: Victor Koteliansky, Skolkovo Institute of Science and Technology, Skolkovo, Moscow, 121205, Russia.
E-mail: kotelianskiv@gmail.com

time consuming to generate animal models.[14] The majority of studies focusing on protein synthesis in eukaryotes have been performed in yeast and mammalian proliferating cells.[8] While a role for eIF3 in translation initiation has long been established, recent studies implicate individual subunits of the complex in the regulation of diverse cellular processes, including longevity, cancer, and organ development.[12,13,15–18] The eIF3m subunit is absent in budding yeast, and it is conserved from fission yeast to higher eukaryotes.[19] eIF3m plays a critical role in maintaining the structural integrity of the eIF3 complex.[20,21] The gene is essential in mouse, both for embryonic development and homeostasis of the mature liver.[19] eIF3m heterozygous mice were viable; however, they showed reduced organ size and diminished body weight.[19]

The objective of the study was to test whether eIF3m is involved in the regulation of the translation of the subset of mRNAs in the liver. More globally, we were interested to evaluate the *in vivo* biological response to the decrease in the translation initiation by perturbating an essential component of the translational machinery.

To investigate the regulatory network associated with the eIF3m subunit, we used small interfering RNA (siRNA) lipid nanoparticles (LNPs) that are capable of delivering functional siRNA to the liver, in both rodents and non-human primates.[22] This approach enables a rapid evaluation of the biological effects of knockdown of essential genes, such as those involved in translation, in the context of the mature organ, in adult animals.[23–25] Furthermore, by applying various concentrations of siRNA LNPs, it is possible to maintain the desired levels of mRNA and thereby titrate the amount of targeted proteins in cells.[22] Using these methods, we found that: (1) long-term knockdown of eIF3m in mouse liver results in the global inhibition of translation and is lethal; (2) the earlier hepatic response (9 and 13 days of treatment with siRNA LNPs) to eIF3m knockdown is associated with changes in transcription but not translational efficiency for individual mRNAs—only 6 genes (including the previously identified ferritin light chain *Ftl1*) were found to be translationally regulated in this system; (3) at the transcriptional level, two major cellular processes, ribosome biosynthesis and cellular metabolism, are affected by eIF3m knockdown; (4) major alterations in ribosome biosynthesis involved increased transcription of the ribosomal proteins and inhibition of rRNA processing; and (5) a similar reduction in eIF3m protein levels is associated with the activated mammalian target of rapamycin (mTOR) pathway *in vitro* but not *in vivo*. Altogether, these results provide new insight into the *in vivo* response to perturbation of the translational machinery and further highlight the utility of using siRNA nanoformulations to study *in vivo* biology.

RESULTS

In Vivo Knockdown of eIF3m in Mouse Liver

siRNAs were designed to avoid off-target activity based on the known criteria for siRNA and mRNA binding properties.[25] The candidate 19-mer siRNA sequences were aligned against the RefSeq mRNA database and ranked based on the number of the mismatches in the seed, non-seed region, and mismatches in the cleavage site position.[25–27] In order to choose the most potent duplexes, we performed *in vitro* dose-response analysis for the 10 selected siRNAs, which were ranked best by the computational analysis. The siRNA with the lowest IC_{50} (4.6 pM with a 95% confidence interval of 2.4–8.6 pM) was chosen for further *in vivo* studies (Figure S1A). Transfection of Hepa1c1c7 cells with the selected siRNA for 3 days resulted in 99% knockdown of eIF3m at the RNA level and more than 90% protein reduction (Figures S1A and S1B).

To perform eIF3m knockdown in mouse liver, we used chemically modified siRNA formulated into C12-200 lipid nanoparticles (LNPs), optimized for hepatic delivery.[22] Due to the relatively small size (around 100 nm) and almost neutral zeta potential, C12-200 siRNA-LNPs pass the endothelium layer, separating hepatocytes from blood, and are further internalized by hepatocytes via macropinocytosis, enabling hepatocyte-specific knockdown.[22,23,26] One day after the tail vein injection of eIF3m siRNA LNP at a concentration of 0.5 mg/kg, we observed more than 95% knockdown of eIF3m mRNA (Figure 1A). The silencing was hepatocyte specific and was not observed in kidney, spleen, lungs, and heart (Figure S1C). A single injection with siRNA LNPs yielded sustained knockdown for 9 days, followed by slow recovery of mRNA levels (Figure S1D). For long-term experiments, mice were repeatedly injected every 5 days. Western blot analysis confirmed knockdown of eIF3m at the protein level in mouse livers upon treatment and showed the reduction of eIF3m by 65% at day 13 and 75% at day 21 of treatment with eIF3m siRNA LNPs (Figures 1B and S1E).

To select the most informative conditions for analyzing the regulatory network associated with the eIF3m-dependent inhibition of translation initiation, we wanted to choose a time point that would better reflect primary changes in transcription and translation after eIF3m knockdown. Such changes would result from the inhibition of translation initiation through eIF3m depletion but would not be associated with the response induced by liver damage due to the reduction of the total protein synthesis.

We evaluated possible changes in liver functioning by the analysis of factor VII activity in mouse serum, ribosome profiles, serum biochemistry, liver morphology, and immunohistochemistry.

Factor VII is a protein with a short half-life (4–6 h) expressed specifically in hepatocytes and secreted into the blood and, thus, represents a convenient marker of liver functioning that could be monitored in the serum without sacrificing the mouse.[28] We reasoned that the changes in the protein synthesis would affect factor VII activity (either directly as a result of the reduced protein synthesis or indirectly through other processes, such as protein folding, trafficking, and secretion). A modest reduction in factor VII activity was detected 6 days after the first injection; a significant effect (more than 50% reduction) could be seen after 10 days of treatment; at day 21, mice began experiencing significant stress and had to be sacrificed. At that time point, factor VII activity was estimated to be 20%, compared to that in the control (Figure 1C).

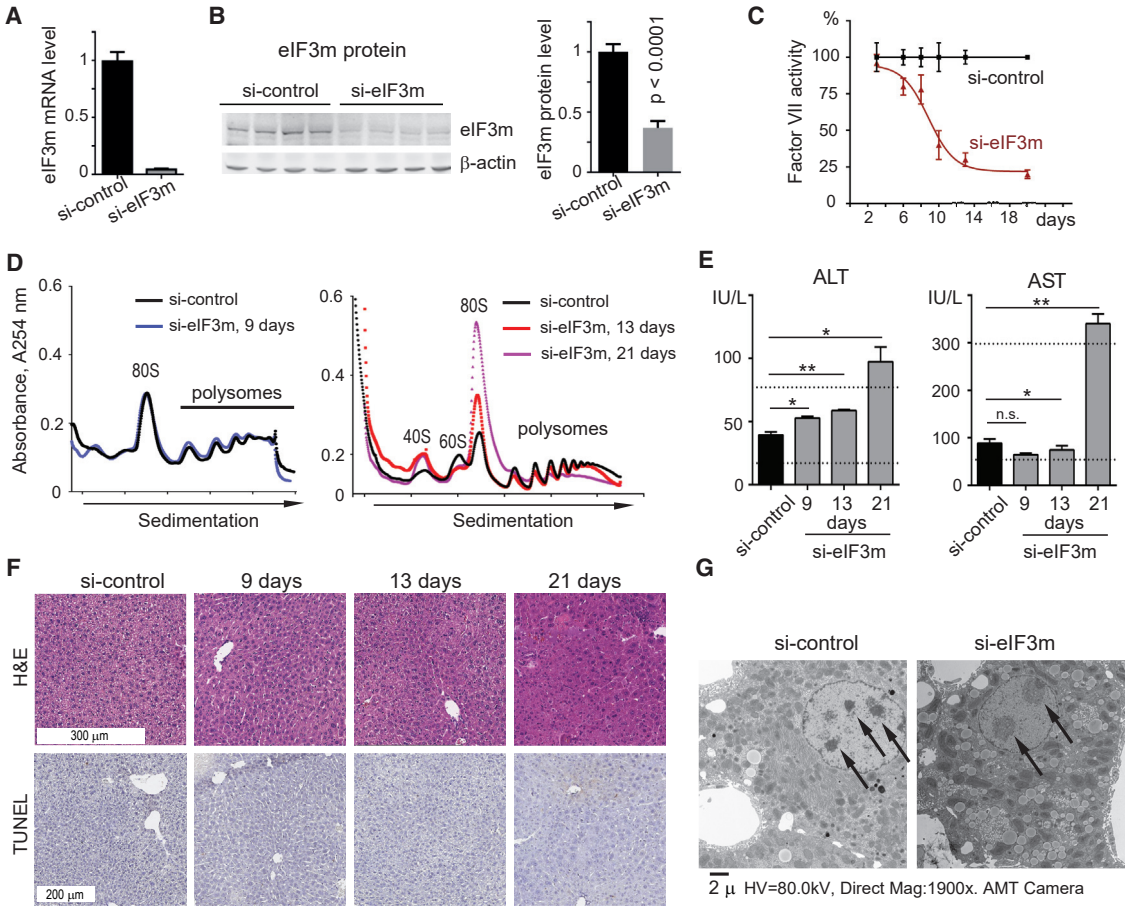

Figure 1. RNAi-Mediated Knockdown of eIF3m in Mouse Liver

(A) eIF3m knockdown at the mRNA level 1 day after injection with siRNA LNPs (0.5 mg/kg, n = 3, mean ± SEM). (B) Western blot analysis of eIF3m protein level in mouse liver 13 days after the first injection with eIF3m siRNA LNPs (n = 4 biological replicates for each condition). (C) Time-course analysis of factor VII activity in mouse serum. (D) Representative polysome profile of the livers treated with eIF3m siRNA LNPs for 9, 13, and 21 days, compared to the control. (E) Fold change in the level of the markers of liver damage ALT and AST in response to eIF3m knockdown. Dashed lines indicate the normal range of the level of the enzyme (n = 3, mean ± SEM). (F) Histological analysis of livers collected from siRNA-LNP-treated mice. H&E staining of liver sections (scale bar, 200 μM); TUNEL assay analysis of liver sections (scale bar, 500 μM). (G) Representative images of transmission electron microscopy performed on mouse livers 21 days after the first injection with eIF3m siRNA LNPs. Arrows indicate nucleoli; round circles indicate accumulation of small lipid droplets in the cytoplasm. For p values, comparison by two-tailed paired t test was used: *$p < 0.05$; **$p < 0.01$.

Polysome profiles did not show any changes in the polysome and monosome quantity/ratio after 9 days of treatment (Figures 1D and 1E). After 13 days of treatment, we detected a decrease in the amount of polysomes and 60S subunits and an increase in the amount of monosomes and 40S subunits; the overall polysome/monosome ratio was decreased, indicating a modest reduction in protein synthesis (Figure 1D).[29] Analysis of the polysome profiles at the 21-day time point showed a significant reduction in the amount of polysomes and an increase in the amount of monosomes, which suggests global decrease in translation initiation and efficiency of protein synthesis (Figure 1D).

The activity of alanine aminotransferase (ALT) and aspartate aminotransferase (AST), markers of liver damage, was within the normal range at the 9- and 13-day time points and elevated above the normal range in mice treated with eIF3m siRNA LNPs at 21 days (Figure 1E). H&E staining did not reveal any changes in liver morphology after 9 days of treatment (Figure 1F). At day 13, vacuoles in a small number of cells around the central vein could be seen, while the periportal zone appeared to be completely normal (Figures 1G and S1F). Livers treated with eIF3m siRNA LNPs for 21 days were characterized by distorted liver architecture (Figure 1G). Nucleoli appeared to be larger in the hepatocytes of treated livers (Figure S1G). We did not observe an induction of apoptosis in response to eIF3m depletion during the course of the experiment, as shown by the dUTP nick-end labeling assay (TUNEL) (Figure 1G). We further performed transmission electron microscopy of liver sections and found that the cytoplasm of hepatocytes was

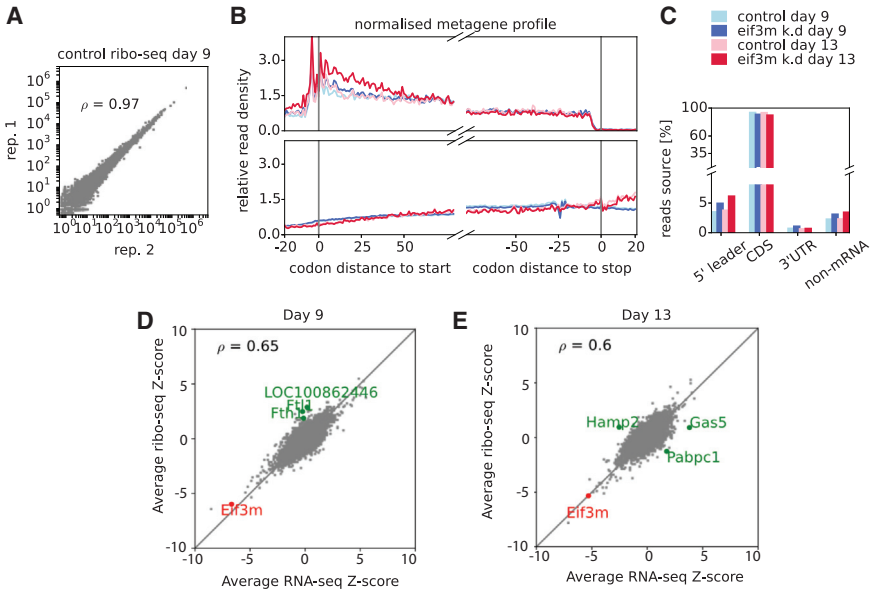

Figure 2. Ribosome Profiling Analysis of Eif3m-Depleted Livers

(A) An example of correlation in the number of aligned reads per gene between two replicates. (B) Meta-gene plots of Ribo-seq (top) and RNA-seq (bottom). (C) Distribution of Ribo-seq reads over different functional regions of mRNAs and to other regions of the transcriptome. (D and E) Analysis of differential gene expression based on changes in RNA-seq signal (x axis) and Ribo-seq signal (y axis) on the 9th (D) and the 13th (E) days. A diagonal line shows the similarity in the response of Ribo-seq and RNA-seq, indicating a general absence of the differential regulation at the translational level. The 6 genes regulated at the translational level are highlighted in green.

vacuolated, with tiny lipid droplets accumulated in the cell (Figure 1H). A similar phenotype is associated with hepatic steatosis.[30] In accordance with the results of H&E staining, livers depleted of eIF3m for 21 days had enlarged, abnormal looking nuclei (Figure 1H).

Based on these results we chose to focus on the analysis of two time points: 9 and 13 days of treatment with siRNA LNPs. These represented two slightly different systems. At 9 days of treatment, liver morphology was completely normal, and there was no change in the polysome-to-monosome ratio; however, the changes associated with the knockdown could be detected based on the factor VII activity assay. At 13 days of treatment, ribosomes were enriched for monosomes, and the amount of polysomes was slightly decreased, indicating reduction in the protein synthesis. This time point was also associated with minor changes in liver morphology (Figures 1G and S1F). We assumed that 9- and 13-day treatment time points would be informative for analysis by RNA sequencing (RNA-seq) and ribosome profiling (Ribo-seq); we further performed proteomic and phosphoproteomic profiling of the livers at the 13-day treatment time point.

eIF3m Knockdown Is Associated with Changes in mRNA Expression and Has Limited Impact on mRNA-Specific Translation

To investigate the effect of eIF3m knockdown on the hepatic transcriptome and translatome *in vivo*, we performed RNA-seq and Ribo-seq analysis of the livers from mice treated with eIF3m or control siRNA LNPs for 9 and 13 days. The Spearman correlation coefficients between the number of aligned reads per gene in all replicates exceeded 0.93, indicating high reproducibility (Figures 2A and S2A).

The metagene profile revealed an increased ribosome density in the 5′ leader and in the first 25 codons of the gene coding sequence (CDS) on day 13 relative to both the controls and treated samples on day 9 (Figures 2B and 2C). This effect was widespread across the analyzed genes and is known to be observed under many stresses.[31,32] The RNA-seq metagene profile showed a higher read density downstream of stop codons on day 13. This difference was not specific to the treatment and reflected differences in RNA-seq approaches (see Materials and Methods).

Differential expression analysis was carried out by means of a *Z*-score transformation, as previously demonstrated.[32] This approach accounts for the variance in dispersion of the gene expression signal owing to differences in the sequencing depths for individual transcripts. We performed the *Z*-score transformation for each replicate (see Materials and Methods) and then used the *Z* scores across the replicates to score the likelihood that RNA levels (through RNA-seq), protein synthesis rates (through Ribo-seq), or translational efficiency (TE; the ratio of Ribo-seq to RNA-seq) was different between the two conditions.

Differential expression analysis confirmed the knockdown of the eIF3m gene (Figures 2D and 2E). It also revealed a significant transcriptional response occurring by day 9, with 575 genes found to be differentially expressed (DE) (false discovery rate [FDR] < 0.05): 246 genes were upregulated, and 329 genes were downregulated (Data S1). A total of 638 genes were differentially expressed at the RNA level upon 13 days of treatment with siRNA LNPs (359 upregulated and 279 downregulated) (Data S1). The transcriptional response at both time points was similar (Spearman's rho = 0.4), with 166 common DE genes between day 9 and day 13 (Figure S2B). The difference in the response indicates a continued reprogramming of gene expression in response to eIF3m knockdown. While the direction of the difference in expression was the same for most of the genes, we detected 8 cases of upregulation at day 9 followed by downregulation at day 13 (Errfi1, Saa3, Ccr1, Lyz1, LOC105244195, Ccrn4l, Col3a1, and Noct) and 2 cases of downregulation at day 9 followed by upregulation at day 13 (Egr1 and Zc3h6).

Further analysis revealed 902 and 835 DE genes at the Ribo-seq level (at days 9 and 13 of treatment, respectively). There was a strong

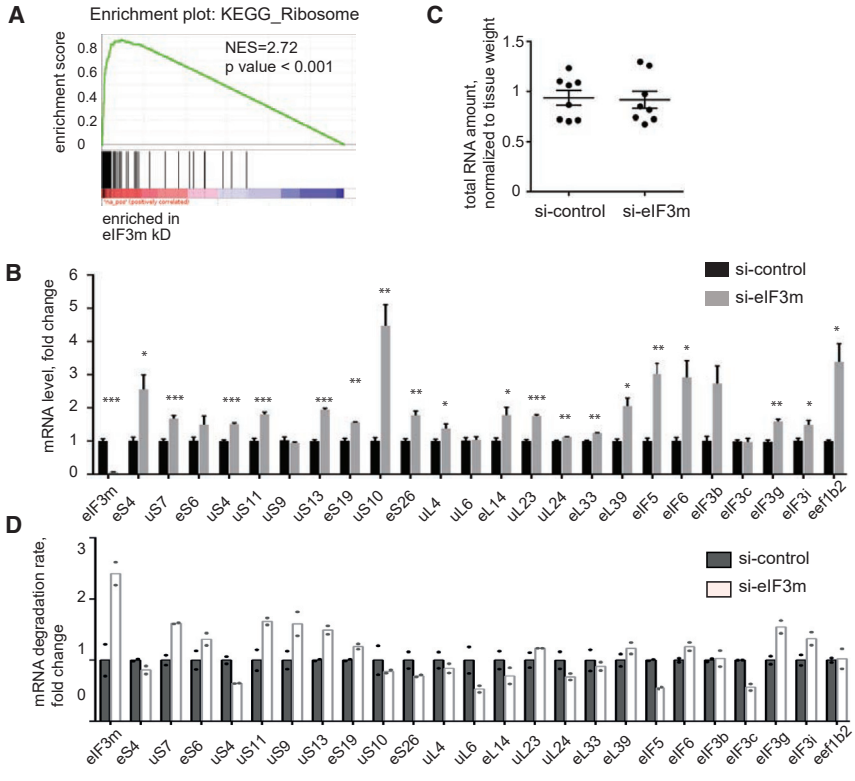

Figure 3. Overexpression of the Genes Involved in Ribosome Biogenesis in Response to eIF3m Knockdown Is a Transcription-Driven Process

(A) Gene set enrichment analysis (GSEA) of the RNA-seq data obtained for liver samples treated with siRNA LNPs for 9 days shows enrichment of the KEGG_Ribosome gene set in eIF3m-knockdown samples. (B) qPCR analysis of the mRNA expression level of the genes involved in ribosome biogenesis in Hepa1c1c7 cells treated with control or eIF3m siRNA LNPs (n = 3 or 4, mean ± SEM). For p values, comparison by two-tailed paired t test was used: *p < 0.05; **p < 0.01, ***p < 0.001. (C) Total RNA amount, normalized by wet tissue weight; livers were collected from mice treated with siRNA LNPs for 13 days (n = 8, mean ± SEM). (D) mRNA degradation rate of the genes involved in ribosome biogenesis in Hepa1c1c7 cells treated with control or eIF3m siRNA LNPs, fold change (experiment performed in biological replicates; individual values are indicated). Universal protein names are used according to Ban et al.[64]

correlation between RNA-seq and Ribo-seq *Z* scores for both time points, indicating that the majority of the changes observed at the level of Ribo-seq is owing to the changes at the RNA level (Figures 2D and 2E). In addition, the comparison of the TE *Z* scores obtained for individual replicates did not reveal evidence of a translational response of specific mRNAs (a general translational repression observed via ribosome profiles would not be detectable with this approach) (Figure S2C).

Only (3 and 3) genes were found to be differentially expressed at the TE level for day 9 and day 13 of the treatment, respectively. The TE DE genes consisted of the upregulation of *LOC100862446*, *Ftl1*, and *Fth1* on day 9 and the downregulation of *Gas5* and *Pabpc1* and upregulation of *Hamp2* on day 13 (Figures 2D and 2E). Interestingly, of the 6 TE DE genes, 4 (light- and heavy-chain ferritins *LOC100862446*, *Ftl1*, *Fth1*, and hepcidin *Hamp2*) belong to the iron metabolism pathway.

We have further performed a western blot against ferritin proteins, which showed a small but significant 10% increase in the expression of Ftl1 protein and a non-significant increase in the expression of Fth1 (Figure S3). The *LOC100862446* gene is an ortholog of *Ftl1*, so it would also be detected as *Ftl1*. Recently, it has been shown that eIF3 acts as a repressor of *Ftl1* translation *in vitro*.[33] Our results confirm the link between eIF3 and Ftl1 and, for the first time, provide evidence for the repression of *Ftl1* translation by eIF3 *in vivo* in the liver.

Transcriptome Changes in eIF3m-Depleted Livers

To gain biological insight into the pathways affected by eIF3m depletion, we performed gene set enrichment analysis (GSEA) using the KEGG gene set collection from MsigDb.[34,35] Analysis of the 9-day time point identified three significantly enriched (FDR q value < 0.05) gene sets in eIF3m-depleted livers (ribosome, extracellular matrix [ECM] receptor interaction, and cell adhesion) and a number of gene sets enriched in the control (Table S1). The two leading gene sets enriched in the control were related to metabolism by cytochrome P450; others represented metabolic pathways, including redox processes and lipid, amino acid, and sugar metabolism. Analysis of the 13-day treatment time point revealed upregulation of the genes involved in 4 KEGG pathway gene sets: ribosome, RNA degradation, spliceosome, and aminoacyl tRNA biosynthesis; 47 gene sets were enriched in the case of downregulated proteins, and many of these were involved in drug metabolism, lipid, amino acid metabolism, and oxidation processes (Table S1). Changes in the gene expression were verified by qPCR analysis for a subset of genes from the KEGG_Ribosome and KEGG_DRUG_METABOLISM_CYTOCHROME_P450 gene sets (Figures S4A and S4B). The result was further reproduced *in vitro* for the genes involved in ribosome biogenesis in Hepa1c1c7 cells treated with eIF3m siRNA LNPs for 3 days (Figure 3).

Overexpression of the Genes Involved in Ribosome Biogenesis in Response to eIF3m Knockdown Is a Transcription-Driven Process

It has previously been shown that the expression of the genes coding ribosomal proteins is coordinated at both the transcription and translation levels. Usually, cells respond to stress by downregulating genes involved in ribosome biogenesis.[36–38] Surprisingly, eIF3m knockdown led to robust overexpression of the ribosomal genes (Figures 3A and 3B). At the same time, we detected no difference in the total RNA content in livers of control and knockdown mice at day 13 (Figure 3C, normalized by wet tissue weight). In order to prove that the increased expression of

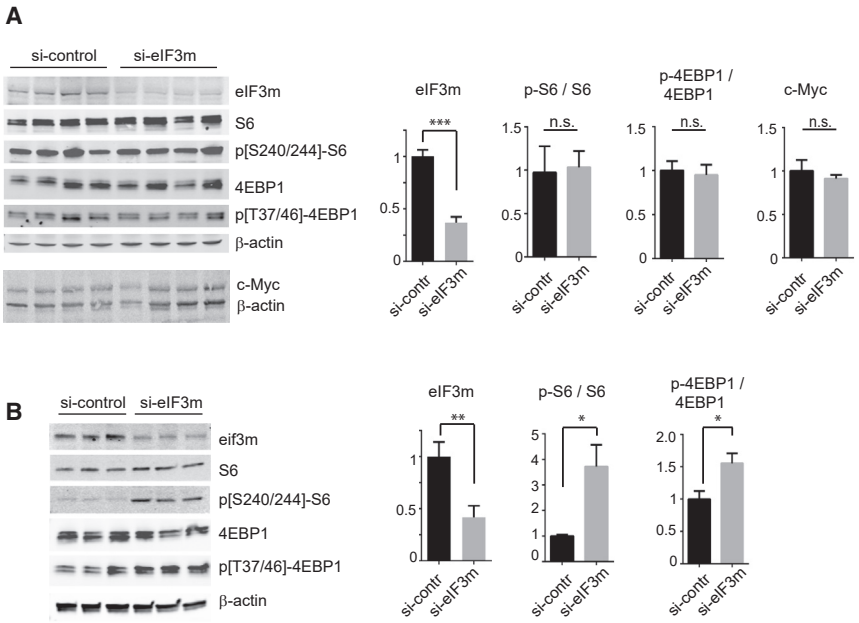

Figure 4. Similar Levels of eIF3m Knockdown Lead to Activation of the mTOR Pathway *In Vitro*, but Not *In Vivo*

Western blot analysis of the phosphorylation status of mTOR targets S6 and 4EBP1. (A and B) Analyzed samples are (A) livers collected from animals treated with siRNA LNPs for 13 days and (B) Hepa1c1c7 cells treated with siRNA LNPs for 3 days. Data represent mean ± SEM. n = 3. For p values, comparison by two-tailed paired t test was used: *p < 0.05; **p < 0.01; ***p < 0.001; n.s., not significant.

the ribosomal genes is caused by eIF3m reduction and not off-target activity of the siRNA, we performed eIF3m knockdown with the 2nd eIF3m siRNA duplex identified during the initial screen. The qPCR analysis confirmed robust upregulation of the ribosomal gene expression in Hepa1c1c7 cells upon treatment with the two different eIF3m siRNAs (Figure S4C), indicating that this effect is a consequence of eIF3m knockdown and not the result of siRNA off-target activity.

The increased abundance of the mRNA of ribosomal genes could be a consequence of increased transcription or inhibited mRNA degradation. In order to distinguish between these possibilities, we evaluated the mRNA degradation rate in a pulse-chase experiment with the use of 4-thiouridin *in vitro*. Briefly, Hepa1c1c7 cells were labeled with 4-sU for 1 h, the medium was then replaced with a fresh one, and labeled RNA was extracted at two time points. The ratio between the remaining labeled RNA at two time points in eIF3m-knockdown cells compared to control cells would, thus, represent changes in the degradation rate.[39,40] As expected, eIF3m mRNA degraded approximately 2.6-fold faster in the eIF3m siRNA-treated cells compared to control cells (Figure 3D). We further assessed degradation rates for the upregulated genes with the most altered expression including 17 ribosomal proteins (10 Rps and 7 Rpl) and 7 translation initiation factors. The fluctuations in mRNA stability were random, with no common direction for the changes between the different genes. Thus, we concluded that increased mRNA levels of the genes involved in ribosome biogenesis are a consequence of the increased transcription and not a subject of a unified mRNA stability regulation mechanism.

A Similar Reduction in eIF3m Protein Levels Is Associated with the Activated mTOR Pathway *in vitro* but Not *in vivo*

Although particular transcription factors, which mediate transcription of ribosomal proteins in mammalian organisms, are not known, it has been shown that c-Myc overexpression is associated with the induction of ribosomal protein genes in mouse liver.[41] We tested c-Myc expression by western blot analysis of the mouse livers and did not detect significant changes in the c-Myc protein level. mTOR is the master regulator of growth, and it has previously been implicated in both transcriptional and translational regulation of the genes involved in protein synthesis.[42,43] We evaluated mTOR pathway activity by analyzing the phosphorylation status of the major downstream mTOR targets S6 and 4EBP1. No changes in the phosphorylation levels of S6 and 4EBP1 proteins were found in mouse liver samples in the tested conditions (Figure 4A). Interestingly, a similar reduction in eIF3m concentration *in vitro* resulted in the significant increase in the phosphorylation of S6 and 4EBP1, indicating strong activation of the mTOR pathway (Figure 4B). Considering that the dynamics of mTOR activation can be different *in vitro* and *in vivo*, we tested other time points *in vitro* (1 and 2 days) and *in vivo* (3 and 9 days). None of the tested *in vivo* samples showed changes in the phophorylation of S6 and 4EBP1, while all of the tested time points *in vitro* showed a significant increase in S6 and 4EBP1 phosphorylation (Figure 4B; Figure S5). Based on these results, we conclude that mTOR is regulated differently *in vitro* and *in vivo* upon knockdown of eIF3m. Further, the absence of changes in the activity of c-Myc and the mTOR pathway *in vivo* suggests that the ribosomal gene expression upon eIF3m knockdown is regulated through a different mechanism.

Proteomic Profiling of eIF3m-Depleted Liver

To assess the relative abundance of proteins in eIF3m-depleted livers, we applied Tandem Mass Tag (TMT) label-based quantitative mass spectrometry. 2,055 proteins were detected, with at least two unique peptides present in all six samples. We found that 174 out of 2,055 detected proteins were differentially expressed (adjusted p value < 0.05). Seven proteins were upregulated with a fold change (FC) >1.5, and 19 proteins were downregulated with an FC >1.5. 74 proteins were moderately upregulated, and 74 were downregulated (1 < FC < 1.5, p < 0.05) (Table S2). The observation of the relatively small changes in protein abundance confirmed that the chosen time point for the experiment reflected primary changes associated with eIF3m knockdown. We used the PANTHER classification system to characterize

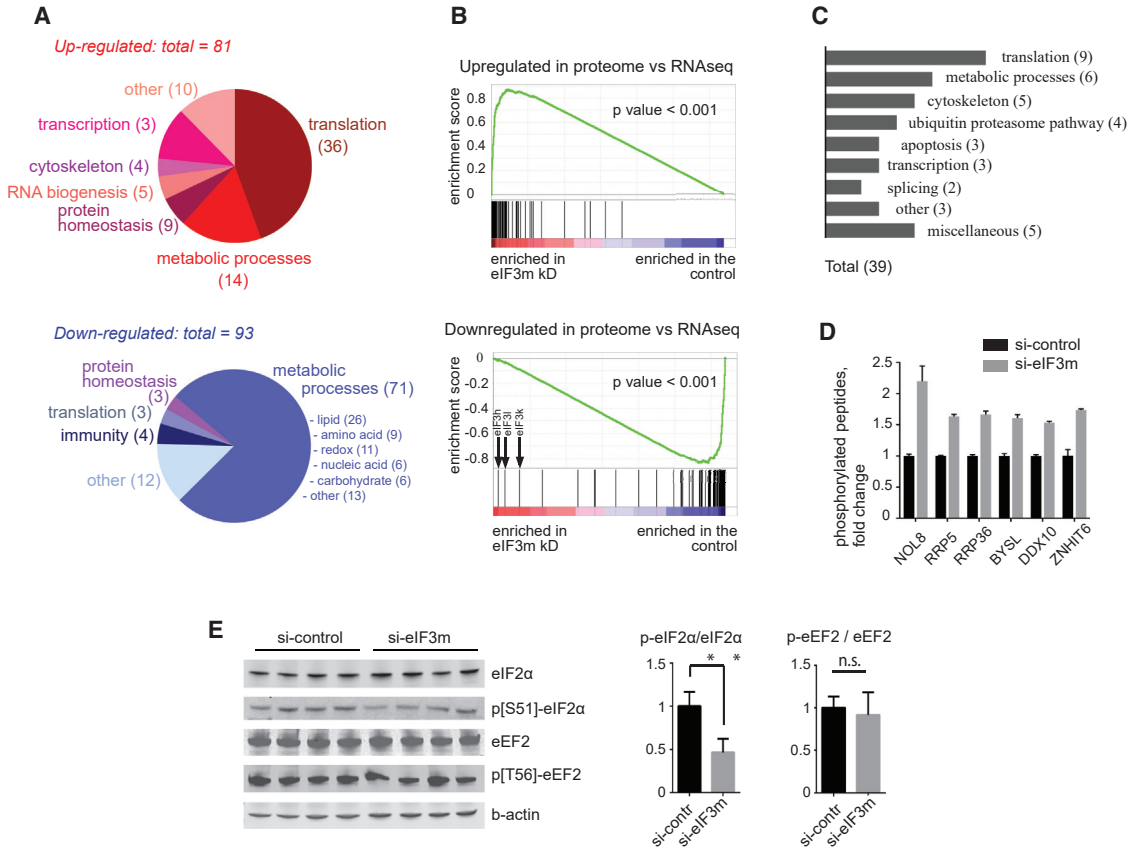

Figure 5. Proteomic and Phosphoproteomic Profiling of eIF3m-Depleted Mouse Livers

(A) Functional classification of differentially expressed proteins. (B) GSEA enrichment plots characterizing the distributions of DE proteins versus mRNA differential expression results where genes higher in eIF3m are indicated on the left (red) and those higher in control are indicated on the right (blue). kD, knockdown. (C) Functional classification of the DE phosphorylated proteins. (D) Fold change level of the abundance of the phosphorylated proteins involved in the rRNA processing. (E) Western blot analysis of the phosphorylation status of the eIF2α and eEF2 translation factors. For p values, comparison by two-tailed paired t test was used: *p < 0.05; **p < 0.01; n.s., not significant.

processes affected upon eIF3m depletion at the proteomics level.[44,45] Consistent with RNA-seq and Ribo-seq data, we observed a 20%–50% increase in the abundance of ribosomal proteins (Figure 5A; Figure S6A; Table S2). Other pathways that described overrepresented upregulated proteins included metabolic processes (in particular, lipid and amino acid metabolism), protein homeostasis, RNA processing, and cytoskeleton maintenance. Pathways that represented downregulated proteins included metabolic processes, protein homeostasis, and transcription regulation (Figure 5A; Table S2).

Differentially expressed proteins were strongly associated with the corresponding condition in mRNA expression data. All genes were ranked from high in Eif3m knockdown to high in control using the Wald statistic from DESeq2 differential expression analysis. Custom gene sets were then prepared from upregulated and downregulated proteins, and GSEA was used to characterize the distribution of these differentially detected proteins in the rank-ordered gene list. In each case, the proteomics-based gene sets were significantly enriched in their corresponding condition in the mRNA-derived contrast. GSEA assigns genes responsible for the observed enrichment to a subset called the leading edge. In this analysis, 58 out of 81 upregulated proteins and 72 out of 93 downregulated proteins are assigned to their corresponding leading-edge groups (Figure 5B). Notable exceptions to these associations are the eIF3h, eIF3k, and eIF3l subunits that were significantly downregulated in the proteome dataset (FCs = 1.44, 1.4, and 1.29, respectively) but were upregulated at the RNA level (FCs = 2.1, 1.3, and 1.4, respectively) (Figure 5B, arrows; Table S2). Previous studies showed that the eIF3m subunit stabilized the eIF3 complex.[19] Thus, it is likely that eIF3m depletion led to the decreased stability of eIF3h, eIF3k, and eIF3l proteins, which would explain the discrepancy between proteome and transcriptome data. We further looked at the protein level of the other eIF3 subunits and found that the abundance of 11 out of 12 subunits was slightly decreased (Figure S6B). Interestingly, the eIF3j subunit protein level was upregulated in eIF3m-depleted liver samples by 1.38-fold.

In summary, the comparison of the differential protein levels with the RNA-seq data suggested that eIF3m knockdown in mouse liver is not

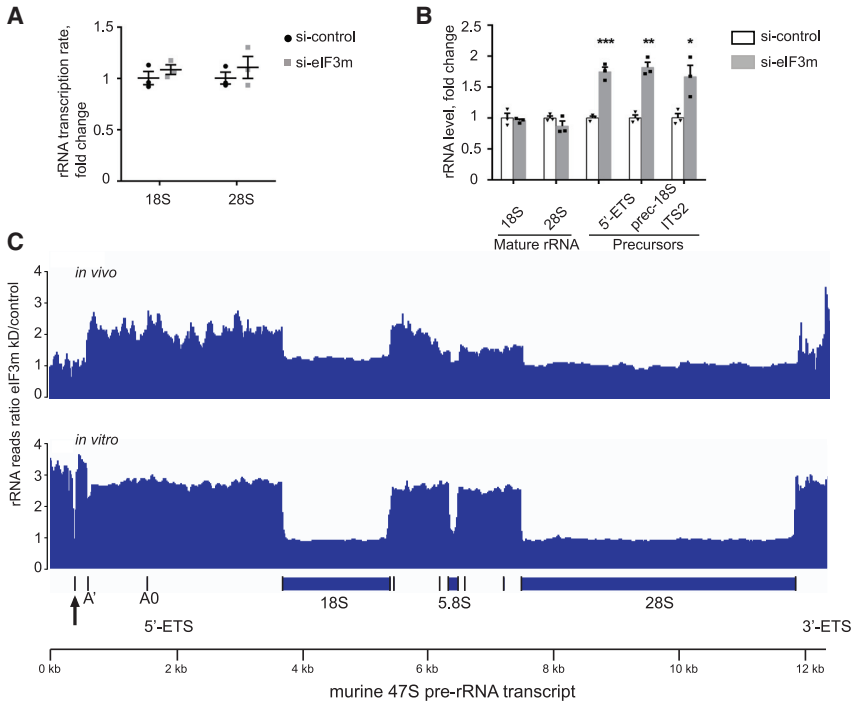

Figure 6. eIF3m Knockdown Affects rRNA Biogenesis

(A) Fold change of the transcription rate of 47S pre-rRNA, assessed by qPCR analysis of 4sU-labeled RNA purified from mouse livers (primers targeting 18S and 28S rRNA) (n = 3, mean ± SEM). (B) Total abundance of the mature and precursor rRNA forms in mouse livers after 13 days of treatment with siRNA LNPs, assessed by qPCR (n = 3, mean ± SEM). (C) Deep-sequencing analysis of 47S pre-rRNA transcript *in vivo* and *in vitro*. Plot represents the ratio between the reads aligned at each position of pre-rRNA in eIF3m knockdown and control livers (n = 3; see Materials and Methods for the details of the analysis and visualization). For p values, comparison by two-tailed paired t test was used: *p < 0.05; **p < 0.01; ***p < 0.001.

associated with changes in TE for a subset of mRNAs at the chosen time points and, thus, confirmed the results of the ribosome profiling analysis.

Phosphoproteome Analysis of eIF3m-Depleted Livers

To understand the broad regulatory network associated with the inhibition of translation initiation *in vivo*, we performed phosphoproteomic profiling of the livers of mice treated with siRNA LNPs for 13 days. The analysis identified 3,458 phosphopeptides on 1,622 proteins. We found 45 phosphopeptides on 39 proteins that showed variation in abundance with 80% confidence intervals; 39 phosphopeptides were upregulated, and 6 were downregulated (Table S3). The identified proteins belonged to the pathways associated with translation, metabolism, the cytoskeleton, the ubiquitin proteasome pathway, apoptosis, transcription, and splicing (Figure 5C; Table S3). Out of the 39 proteins, 6 upregulated proteins were involved in rRNA biogenesis (NOL8, RRP5, RRP36, BYSL, DDX10, and ZNHIT6) (Figure 5D).

In addition to the identified proteins, we were interested in the phosphorylation status of the translation factors eEF2 and eIF2alpha, as their phosphorylation plays an important role in the regulation of translation in response to diverse stimuli. eIF2 recycling is an important step of translation initiation; phosphorylation of the alpha subunit of eIF2B factor inhibits recycling and, thus, leads to a decrease in global protein synthesis.[46] Western blot analysis showed a 20% decrease in the phosphorylation of the eIF2alpha subunit (Figure 5E). Such a modification would favor an increase in the efficiency of translation initiation.[46] eEF2 phosphorylation is another major pathway regulating translational efficiency, which is often activated in response to stress.[47] No difference in eEF2 phosphorylation was detected in eIF3m-depleted livers after 13 days of treatment (Figure 5E).

rRNA Processing Is Altered in eIF3m-Depleted Liver and Cultured Hepa1c1c7 Cells

The increased amount of the phosphorylated proteins involved in rRNA biogenesis encouraged us to assess rRNA maturation (transcription rate and processing) in the eIF3m knockdown system.

Four rRNA molecules constitute the core of the eukaryotic ribosome. 18S, 5.8S, and 28S rRNAs are synthesized by RNA polymerase I as a long polycistronic precursor (47S), which matures through a coordinated series of cleavage steps; 5S is transcribed by RNA polymerase III. After the processing, the non-coding regions of the rRNA precursor quickly degrade, while mature rRNAs assemble with the ribosomal proteins and are exported into the cytoplasm.[48]

We first checked whether the activity of polymerase PolI (transcription rate of 47S rRNA precursor) was affected. Mice treated with siRNA for 12 days were injected with 4-thiouridin; 24 h later, newly synthesized labeled RNA was purified via conjugation with biotin followed by isolation on magnetic beads; relative quantities of 18S and 28S rRNA were then assessed by qPCR. No changes in the transcription rate of 47S pre-rRNA was detected (Figure 6A). This result was reproduced *in vitro* in Hepa1c1c7 cells (Figure S7A).

We further assessed the total abundance of rRNA upon eIF3m depletion *in vitro* and *in vivo* using qPCR. In both cases, there were no significant changes in the qPCR signal for 18S and 28S rRNA; however, we detected an approximately 1.6-fold increase in the abundance of rRNA precursors (Figures 6B and S7B). Such a result indicates an inhibition of the processing of the 47S rRNA precursor.[49] Indeed, since the rRNA transcription rate was not affected, the cell would produce the same quantities of rRNA, resulting in similar qPCR estimates for the mature 18S, 28S, and 5S sequences. However, inhibition of rRNA

processing would result in reduced degradation of the pre-rRNA external and internal spacers, which would lead to an increase in their abundance in eIF3m-depleted cells.

Through the analysis of H&E liver staining and transmission electron microscopy, we observed enlarged nucleoli in eIF3m-depleted livers at the 20-day treatment time point (Figures 1G and S1G). Such an effect was in agreement with the inhibited rRNA processing, as unprocessed rRNA cannot be exported from the nucleus and, thus, accumulates in the nucleoli.

To gain further insight into the particular steps of rRNA processing affected in eIF3m-depleted hepatocytes, we performed deep sequencing of rRNA transcripts from the *in vivo* (13-day treatment time point) and *in vitro* (3-day treatment of Hepa1c1c7 cells) experiments. Sequencing reads were aligned to the 47S rRNA precursor. The depth of coverage was quantified with SAMtools (v.1.3). Figure 6C shows the ratio between the number of rRNA reads in eIF3m versus control siRNA-treated samples. Sequencing showed an approximately 2- to 3-fold increase in the abundance of the non-coding areas of rRNA within the 5′ ETS, ITS1, ITS2, and 3′ ETS segments of 47S pre-rRNA. This observation is consistent with the qPCR measurements and supports the conclusion of inhibited rRNA processing. The ratio between the reads corresponding to the mature 18S, 5.8S, and 28S was close to 1, which confirms that the rate of rRNA transcription remained unchanged, both *in vitro* and *in vivo*. At the chosen time points, we observed several differences between *in vivo* and *in vitro* data. The ratio of the reads aligned to the pre-rRNA area 1–650 nt (A' site) remained unchanged *in vivo*; however, *in vitro*, this segment was enriched 3- to 3.5-fold in eIf3m-depleted cells. The result suggested uncoupling of the A' site from the other processing steps *in vivo* but not *in vitro*.

Further, we observed a gap in the eIF3m/control reads ratio at position 414–447 nt *in vitro* (Figure 6C, arrow; Figure S7C), which most likely indicates an rRNA processing step in this region. The gap was not seen *in vivo*, suggesting a difference in the regulation of rRNA processing in the developed system in liver and Hepa1c1c7 cells. The region C414-C416 to G420-U422 has previously been identified as the cleavage site for human pre-rRNA (site 01) but not mouse.[48]

In summary, our data indicate the inhibition of rRNA maturation in response to eIF3m knockdown and further suggest differences between the *in vitro* and *in vivo* regulation of rRNA processing (the A' cleavage site remains active *in vivo* but not *in vitro*; additionally, rRNA sequencing data *in vitro* provides evidence of the human 01 processing site, which has not been previously reported in mouse pre-rRNA).

DISCUSSION

Despite advances in understanding protein synthesis in yeast and mammalian proliferating cells, less is known about the regulation of translation in adult tissue *in vivo*.[8] One challenge is the lack of methods available to study ribosomal factors *in vivo*, as knockout of many key translation genes leads to lethality at different stages of embryogenesis.[2,19] Conditional deletion of ribosomal proteins in adult animals and heterozygous knockout mice represents one way of dissecting the role of translation factors. Nevertheless, genetic manipulations are costly, time consuming, and require animal breeding and colony maintenance. *In vivo*, RNAi overcomes these limitations by enabling rapid experimental design, the selection of any available mouse strain, and the combinatorial targeting of more than one gene at a time.[50,51] This experimental flexibility allows for more rapid dissection of complex translation-related genetic disorders, such as ribosomopathies.[52,53] Furthermore, the success of siRNA LNPs in the clinic may allow for rapid extension of gene knockdown targets into human trials.[54] Most importantly, siRNA LNP-based knockdown allows for the assessment of hepatocyte biology *in vivo* in the context of the mature liver.

Multiple steps need to be coordinated to generate and assemble ribosomes on mRNA, including transcription and processing of rRNA, transcription and translation of ribosomal proteins and translation factors, export of the ribosomal subunits from the nucleus, and assembly of the ribosome with mRNA in the cytoplasm.[29,53,55] Eukaryotic initiation factor eIF3, a complex consisting of 13 subunits (eIF3a to eIF3m), is one of the largest participants in the translation machinery. Growing evidence suggests that, apart from the general role of eIF3 in initiating cap-dependent translation, it can specifically regulate expression of the subset of genes at the translational level.[13,16–18]

One of the objectives of the study was to test whether eIF3m is involved in the regulation of the translation of specific mRNAs *in vivo* in the liver. We have observed that the reduced concentration of eIF3m led to a significant transcriptional response (Table S1) but only minor changes in the TE for specific mRNAs (Figure 2). Only 6 genes were identified to be translationally regulated in the eIF3m-treated livers. Interestingly, 4 out of the 6 identified genes are involved in the iron metabolism pathway (light- and heavy-chain ferritins *LOC100862446*, *Ftl1*, and *Fth1* and hepcidin *Hamp2*). Recent research provides an additional confirmation for the link between eIF3 and ferritin genes.[33] Previously, photoactivatable ribonucleoside-enhanced crosslinking and immunoprecipitation (PAR-CLIP) analysis showed interaction between ferritin light-chain (FTL) mRNA and eIF3 subunits.[16] It has further been shown that eIF3 acts as a repressor of FTL mRNA translation and that eIF3-mediated *Ftl* repression is disrupted by a subset of SNPs in the FTL 5′ UTR that cause hyperferritinemia, a disease characterized by an overload of ferritin protein in the liver.[33,58] Our finding of eIF3m knockdown leading to increased *Ftl1* translation efficiency is in agreement with these data; it also, for the first time, provides justification for the link between eIF3 and ferritins *in vivo* in the liver.

It is possible that there are more genes regulated at the level of the translation in response to eIF3m knockdown; however, they could not be identified, as some of the changes in mRNA level relate to mRNA stability changes caused by translation. The importance of the coupling of mRNA stability and translation has become

increasingly clear, at least in yeast, in recent years.[56,57] It is also possible that the reduced eIF3m level causes mostly a general effect on translation of all mRNAs in the cells, which is not specific to particular mRNAs (except for the discussed genes).

We demonstrated that the decreasing concentration of eIF3m led to differential regulation of several steps of the ribosomal biosynthesis process (the scheme is shown in Figure S8). eIF3m depletion was followed by the increased transcription of ribosomal proteins (Figure 3; Table S1), an increased amount of phosphorylated rRNA biogenesis proteins (Figure 5B), and inhibition of rRNA processing (Figure 6). Furthermore, we detected a decrease in eIF2alpha phosphorylation (Figure 5E), an important regulatory step of the translation initiation process.[9] Similarly to the eIF3m knockdown system, rRNA processing is negatively regulated in starvation conditions and in response to DNA damage both in yeast and in mammalian cells.[49,59,60] Such a response leads to further inhibition of the protein synthesis.[37,60] On the contrary, the increase in the transcription of the proteins involved in translation is rarely detected in response to stress.[36,61] Both increased production of the ribosomal proteins and dephosphorylation of eIF2alpha would favor an increase in global protein synthesis.[35,60] We anticipate that these processes are activated to compensate for the decreased protein synthesis, sensed by the cell (Figure S8). The combination of the global upregulation of ribosomal protein genes and downregulation of rRNA processing indicates decoupling of the major steps of ribosome biosynthesis in response to the inhibition of translation initiation (Figure S8).

rRNA sequencing analysis suggested that rRNA maturation *in vivo* (in the liver) and *in vitro* (Hepa1c1c7 cell culture) is regulated differently in response to eIF3m depletion. Our data indicate that the A' cleavage site remained active *in vivo* but not *in vitro* (Figure 6C). The *in vivo* result is in agreement with previous data, which showed that A' could be uncoupled from the other processing steps under certain types of stress.[48] The earliest processing site previously characterized for murine rRNA precursor is located at the position A650-U652, A656-A658 nt.[48] Interestingly, we detected a gap in the 414- to 447-nt region in the case of eIF3m-depleted cells *in vitro* (Figure 6C; Figure S7C). This position corresponds well to the 01 processing site found in human 47S rRNA (C414-C416 and G420-U422) but has not been described in a mouse pre-rRNA. This result could be explained in two ways. The processing step could be specifically activated upon eIF3m knockdown, which would explain why it has not been characterized previously in murine pre-rRNA. It is also possible that the site is constantly active *in vitro*; however, the fact that it has not been detected in earlier studies argues against this possibility. Importantly, a number of ribosomopathies are associated with the inhibition of rRNA processing in response to depletion of the translation factors.[1]

Interestingly, eIF3m knockdown was associated with the induction of the mTOR pathway *in vitro*, which could not be detected *in vivo* under similar eIF3m protein levels (Figures 4A, 4B, and S5). mTOR is a serine/threonine protein kinase that integrates signals from nutrients, growth stimulation, and stress. It is also known to be a master regulator of protein synthesis, accounting for various changes in the ribosome biogenesis, including rRNA synthesis and ribosomal protein transcription and translation.[62,63] Activation of mTOR *in vitro* is in line with the previous data showing that inhibitors of protein synthesis, such as cycloheximide, can activate mTORC1 through increased intracellular levels of amino acids.[61] The lack of mTOR activation in the *in vivo* data could be associated with the slower dynamics of eIF3m reduction. A similar level of eIF3m knockdown at the protein level (approximately 60% protein reduction) was detected after 3 days *in vitro* and 13 days *in vivo* (Figures 4A, 4B, and S5). It is possible that the slower protein knockdown dynamics *in vivo* allows the system to adjust to the protein expression changes without mTOR activation.

The detected differences in the rRNA processing and in mTOR pathway activity *in vitro* and *in vivo* highlight the importance of working with the animal models for studying different aspects of translation regulation. Accumulating such knowledge will be important to understand molecular mechanisms that involve dysregulation of the protein synthesis in response to stress and diseases.

MATERIALS AND METHODS

Cell Culture

The following siRNAs were used: lead eIF3m sense, 5′-uGAuAA AGAuGuuGAAAGudTsdT-3′; lead eIF3m antisense, 5′-ACUU UcAAcAUCUUuAUcAdTsdT-3′; control sense, 5′-cuuAcGcuGAG uAcuucGAdTsdT-3′; and control antisense, 5′-UCGAAGuACUc AGCGuAAGdTsdT-3′. 2′-OMe-modified nucleotides are indicated with lowercase letters, and phosphorothioate linkages are indicated by the letter "s." siRNAs were formulated in LPNs, as described by Love et al.[22] Hepa1c1c7 cells obtained from ATCC were propagated in DMEM supplemented with 10% fetal bovine serum (FBS). Cells were transfected either with siRNA using Lipofectamine RNAiMAX (Invitrogen) or with siRNA LNPs.

Animals

FVB/N mice were purchased from Charles River Laboratories. Study protocols were approved by the Committee on Animal Care of MIT. Six- to 8-week-old mice received siRNA in LNP formulations at 0.5 mg/kg via tail vein injection (intravenously [i.v.]). Blood for analysis was collected from submandibular vein via the cheek pouch method. Factor VII activity in the blood serum was measured with the Biophen Factor VII assay (HYPHEN BioMed). Animals were sacrificed by CO_2 overdose.

Histological and Immunohistochemical Analyses

Freshly collected liver tissues were fixed in 4% buffered paraformaldehyde and embedded into paraffin. Sections (5 μm thick) were subjected to H&E or TUNEL staining. The EnVision System (Dako) was used for indirect peroxidase reaction, with 3,3'-Diaminobenzidine (DAB) used as a chromogen.

Electron Microscopy

The liver tissue was trimmed and fixed in 2.5% gluteraldehyde, 3% paraformaldehyde with 5% sucrose in 0.1 M sodium cacodylate buffer

(pH 7.4) and post-fixed in 1% osmium in veronal-acetate buffer. The tissue was stained in block overnight with 0.5% uranyl acetate in veronal-acetate buffer (pH 6.0) and then dehydrated and embedded in Embed-812 resin. Sections were cut on a Leica Ultracut UCT microtome with a Diatome diamond knife at a thickness setting of 50 nm and were stained with uranyl acetate and lead citrate. The sections were examined using an FEI Tecnai Spirit transmission electron microscope at 80 kV.

Gene Expression Analysis by qPCR

Gene expression analysis was performed by qPCR using the Roche LightCycler 480. Gapdh or β-actin mRNA were used as housekeeping gene controls. The mRNA levels were normalized to the housekeeping gene level and to an average value in the control group. Specific probes and primers are listed in Table S4.

RNA Sequencing and GSEA

RNA for sequencing was purified from frozen ground livers with the use of the QIAGEN RNeasy Mini Kit. Single-end RNA-seq reads were aligned to mm10 with STAR v.2.5.3a, and gene expression was summarized with RSEM v.1.3.0 using an Ensembl v.88 annotation. Differential expression analysis was done using DESeq2 v.1.18.1 without fold change moderation and with Cook's cutoff and independent filtering turned off. The DESeq2 Wald statistics were used as the ranking metric in pre-ranked GSEA with the KEGG gene set collection from MsigDB v.6.1 or custom gene sets prepared from proteins found to be differentially expressed using proteomics analysis.

Ribosome Profiling

Polysome profiles were obtained from 20 mg frozen liver. The tissue was pulverized with a ceramic mortar and pestle filled with liquid nitrogen and then lysed using a glass Teflon Dounce homogenizer in a lysis buffer: 20 mM Tris-HCl (pH 7.5), 100 mM KCl, 5 mM $MgCl_2$, 1 mM DTT, 1% Triton, 0.1 mg/mL cycloheximide. Lysate was cleared by a 2-min spindown at 12,000 × g. When the preparative extraction of ribosome-protected fragments was required, heparin was added to a final concentration of 800 μg/mL followed by the addition of 2 μL RNase T1 (Epicenter) and 1 h incubation at room temperature with gentle agitation. Ribosome fractionation was performed by ultracentrifugation for 3 h at 35,000 rpm in an SW41 rotor (Beckman Coulter, Optima L-20K) at 4°C in a 10%–50% sucrose gradient buffered with 20 mM Tris-HCl (pH 7.5), 100 mM KCl, 10 mM $MgCl_2$, 1 mM DTT, 0.1 mg/mL cycloheximide. After the centrifugation, gradients were passed through a UV detector (Bio-Rad), and the absorption at 254 nm was recorded. The fraction containing monosomes was collected in a single tube and concentrated to 50 μL on a 100-kDa filter (Amicon, Millipore). The concentrate was diluted to 600 μL with 10 mM Tris-HCl (pH 7.5), 2 mM EDTA, 1% SDS. Total RNA was extracted by hot acid phenol (Ambion) and precipitated by ethanol (1/10 volume 3M sodium acetate [pH 5.5], 1/100 volume glycogen, 2.5 volumes ethanol 100%, incubated for 1 h at −20°C). RNA was loaded on a 15% Tris-borate-EDTA (TBE)-urea polyacrylamide gel. The band at around 28–30 nt was cut, and RNA footprints were eluted and dephosphorylated with T4 kinase (Fermentas). The sequencing library was prepared similarly to the protocol described in the ARTseq Kit (Epicenter), with some changes. The 3′ adaptor (rApp-AGATCGGAAGAGCACACGTCT-ddC) was ligated to footprints with T4 ligase 2 truncated (New England Biolabs [NEB]): 2.75 μL water, 4 μL 50% PEG 8000, 1 μL ligase buffer, 0.25 μL Superase-In, 1 μL ligase, with 3-h incubation at −25°C. After ligation, reaction was precipitated with ethanol, and a reverse transcription was set up: 11.5 μL ligation product resuspended in water, 1 μL reverse transcription primer, 1 μL dNTP mix (10 mM), with incubation at 65°C, placement on ice, and the addition of 4 μL 5× buffer, 2 μL DTT, 0.5 μL Superase-In, and 0.5 μL SuperScript III (Life Technologies). The reaction was kept for 30 min at 48°C, 1 min at 65°C, and 5 min at 80°C. To get rid of RNA, we added 0.8 μL of 2 M NaOH for hydrolysis and incubated for 30 min at 98°C. The reaction mix was neutralized by 0.8 μL of 2 M HCl and precipitated with ethanol. The pellet was resuspended in 16.5 μL water, and the ligation reaction was set up with the CircLigase II Kit (Epicenter). Ribo-seq libraries were amplified by PCR with individually barcoded primers (Table S5) using Phusion polymerase (NEB).

The analysis was done with 3 replicates per condition in the case of 9-day treatment and 2 replicates per condition in case of 13-day treatment. RNA-seq on day 9 was done with single-end reads 70 nt in length; the sequencing on day 13 was performed using paired-end reads 50 nt in length. Between 7 and 56 million non-rRNA RNA-seq reads and between 1.9 and 9.1 million Ribo-seq reads were mapped for each sample (Table S7). The RNA-seq data analysis was carried out similarly to that of Andreev et al.[32] The reads were clipped with Cutadapt and aligned to the RefSeq annotated transcriptome with Bowtie. The RefSeq annotations were downloaded on June 13th, 2016, and thereby closely correspond to release 77. For the quantification of the Ribo-seq signal of protein coding genes, only those reads were used whose inferred A' site codon locations were mapped to annotated CDS. For transcripts lacking annotated CDS, all the aligned reads were used to quantify expression. The A' site location of footprints was inferred using a 17-nt offset from the read 5′ end. For quantification of gene RNA levels, the RNA-seq reads aligning to all transcripts deriving from the same gene locus were used. Reads that aligned to transcripts from more than 3 genome loci were discarded, while the value of "ambiguous" reads that aligned to 2 or 3 genes was downweighed proportionally (i.e., the count of a read mapped to two genes was reduced by half).

The meta-gene profile was made using read alignments to the longest transcript of each gene, transcripts with 5′ leaders, and 3′ UTRs shorter than 60 nt were excluded as well as transcripts with less than 100 reads aligned to them. The density of footprints was normalized for each transcript by the average read density of its annotated coding region. The normalized densities were aggregated to produce a meta-gene profile. The meta-gene profile shown in Figure 2A is an average of the meta-gene profiles for the individual replicates for each condition.

A *Z*-score transformation was carried out to score the likelihood that RNA levels (RNA-seq), protein synthesis rate (Ribo-seq), or translation

(TE) of the genes were different between the two conditions. In the *Z*-score transformation, genes were first binned into groups of 300 based on the lowest read count of the RNA-seq samples as before.[32] For differential expression of RNA-seq (or Ribo-seq), this is simply the minimum RNA-seq (or Ribo-seq) read count across the two conditions. For differential expression analysis of TE, this is the minimum read count of either Ribo-seq or RNA-seq across the two conditions. The SD and mean difference between the two conditions of the genes in each bin were then used to calculate the *Z* score for each gene. The *Z*-score transformation was performed independently for each replicate.

FDR Calculation

The absolute value of the average *Z* score was used to score the transcript as differentially expressed:

$$z = \left| \frac{\sum_{n=0}^{n=N} Z_n}{N} \right|,$$

where N is the number of replicates and Z_n is the *Z* score in the replicate n. We chose the threshold for calling a transcript differentially expressed based on the empiric FDR, which we determined using the following approach. The *Z* score for every gene may be characterized based on its direction as either positive (+) or negative (−). With multiple replicas or tests, the direction of the *Z* scores of bona fide differentially expressed genes is expected to be the same, e.g., (+/+) or (−/−) for two replicates. However, the difference in expression signal due to technical variation between two replicates is equally likely to be convergent (+/+, −/−) or divergent (+/−, −/+).

The average of the absolute *Z* score may be defined as:

$$z' = \frac{\sum_{n=0}^{n=N} |Z_n|}{N}.$$

We used this value, obtained from divergent genes as a means to estimate the expected distribution of $\bar{z}$. For instance, for two replicates, the number of divergent transcripts exceeding z' can be used to approximate the number of false positives among the genes determined as differentially expressed with z' equal to $\bar{z}$. This principle can be extended to any number of replicates, as the number of convergent transcripts exceeding a certain $\bar{z}$ relates to the number of divergent transcripts (with at least one inconsistent replicate) as $2/(2^n\text{-}2)$ for n replicates. Thus, the FDR for a certain threshold, z', equals the number of divergent transcripts with $\bar{z}$ exceeding the same threshold value multiplied by $2/(2^n\text{-}2)$. We used an FDR of 0.05 as a threshold of differential expression.

Measurement of the Changes in mRNA Degradation Rate in eIF3m-Depleted Cells

3 days after the treatment with siRNA, Hepa1c1c7 cells were labeled with 250 μM 4-sU (Sigma) for 1 h, the medium was then replaced with a fresh one, and total RNA was extracted at two time points (immediately after labeling with 4-sU for 1 h and 4 h after the medium was replaced with a fresh one). 4-sU-labeled RNA was further isolated as previously described.[39] The relative amount of labeled mRNA of the ribosomal protein genes was assessed by quantitative real-time PCR analysis at two time points in control and eIF3m siRNA-treated cells. The ratio between the labeled RNA at two time points in eIF3m knockdown compared to control cells was quantified to assess the changes in the degradation rate.

Western Blot Analysis

Western blot analysis was performed as in the study by Bogorad et al.[23] Antibodies used for the analysis are listed in Table S6.

Proteomic and Phosphoproteomic Analyses of Liver Samples

Liver samples from 3 control and 3 eIF3m siRNA-LNP-treated mice were lysed in 8 M urea (Sigma); protein concentration was quantified using the Pierce BCA Protein Assay Kit. Lysates were reduced with 10 mM DTT and then alkylated with 55 mM iodoacetamide in the dark. Proteins were digested with modified trypsin (Promega) at an enzyme/substrate ratio of 1:50 in 100 mM ammonium acetate (pH 8.9) at 25°C overnight. Trypsin activity was halted by the addition of acetic acid (99.9%; Sigma) to a final concentration of 5%. Samples were further desalted with Protea Biosciences C18 spin columns.

Peptide labeling with TMT 10plex Labeling Reagent (Thermo Fisher Scientific) was performed per the manufacturer's instructions. The TMT-labeled peptide pellet was fractioned via high-pH reverse-phase high-performance liquid chromatography (HPLC) into 15 fractions. The fractions were vacuumed with the SpeedVac vacuum concentrator (Thermo Scientific Savant) to near dryness. In the case of phosphoproteome analysis, phosphopeptides were enriched from each of the 15 fractions using the High-Select Fe-NTA Phosphopeptide Enrichment Kit (Thermo Fisher Scientific) per the manufacturer's instructions. Peptides were loaded on a precolumn and separated by reverse-phase HPLC using an EASY-nLC 1000 liquid chromatograph (Thermo Fisher Scientific) over a 140-min gradient before nanoelectrospray using a QExactive Plus mass spectrometer (Thermo Fisher Scientific). The full mass spectrometry (MS) scan was followed by tandem MS (MS/MS) for the top 10 precursor ions in each cycle with a Normalized Collision Energy (NCE) of 34 and dynamic exclusion of 30 s. Raw mass spectral data files (.raw) were searched using Proteome Discoverer (Thermo Fisher Scientific) and Mascot v.2.4.1 (Matrix Science). Only peptides with a Mascot score greater than or equal to 25 and an isolation interference less than or equal to 30 were included in the data analysis. The p values were quantified with the usage of the limma package for Affymetrix microarrays.

Analysis of rRNA Biogenesis by Sequencing

RNA for sequencing was purified by phenol-chloroform extraction from grinded livers. In the case of Hepa1c1c7 cells, RNA for sequencing was purified with the use of the SurePrep Nuclear RNA Purification Kit from Fisher Scientific. RNA was quantified using the Fragment Analyzer System (Advanced Analytical

Technologies), and 1 ng total RNA was used to prepare indexed RNA-seq libraries using the SMARTer Stranded Total RNA-Seq - Pico Input Mammalian Kit (Takara), omitting the depletion of ribosomal cDNA with the ZapR step. Illumina libraries were quantified using the Fragment Analyzer and by qPCR and sequenced on an Illumina MiSeq using 75-nt paired-end reads. Reads were aligned to the mouse 45S rRNA precursor (GenBank: NR_046233.2) using BWA-MEM v.0.7.12. Sequence depth at each position was then calculated using SAMtools depth v.1.3. The depth at each position was then normalized for sequence volume by scaling each value to correspond to the depth per 10,000,000 total depth for each sample. The normalized depths for each sample group were then averaged and a ratio of Eif3m/Control was calculated for each position. Ratios were then converted to bedGraph format and visualized with IGV v.2.3.

Data Availability

The GEO submission (GEO: GSE118395).

SUPPLEMENTAL INFORMATION

Supplemental Information can be found online at https://doi.org/10.1016/j.omtn.2019.11.009.

AUTHOR CONTRIBUTIONS

E.M.S., M.V.G., T.S.Z., R.L.B., R.L., V.N.G., D.G.A. and V.K. designed the experiments, which were performed by E.M.S., M.V.G., K.J.K., and A.S.F., and analyzed by E.M.S., M.V.G., P.B.O., C.A.W., R.L.B., and P.V.B. Ribo-seq analysis was performed by P.B.O. and P.V.B. E.M.S., M.V.G., P.B.O., P.V.B., D.G.A., and V.K. prepared the manuscript, which was read and approved by all authors prior to submission.

CONFLICTS OF INTEREST

Robert Langer receives licensing fees (to patents for which he was an inventor) from, invested in, consults (or was on scientific advisory boards or boards of directors) for, lectured (and received a fee), or conducts sponsored research at MIT, for which he was not paid, for the following entities : 7th Sense, Abpro, Aleph Farms, Alkermes, Allevi, Alnylam, Artificial Cells, Arsenal Medical, BASF, Celero, Cellomics, Cellular Biomedical, Clarus, Clontech, Combined Therapeutics, Conference Forum, Curis, Domain, Eagle, Echo, Edge, Evox, Fate Therapeutics, Frequency Therapeutics, Gecko Health, GenScript, Glycobia, Glympse, Grandhope, Greenlight, HKF Technologies, Horizon Discovery, Humacyte, Indivor, Inovio, Institute of Immunology, InVivo Therapeutics, Ironwood Pharmaceuticals, Kala, Kallyope, Kensa, Keratinx, KSQ Therapeutics, Landsdowne Labs, Like Minds, Luminopia, Luye, Lyndra, Lyra, Medical Kinetics, Merck, Micelle, Moderna, Momenta, Monsanto, Mylan, Nanobiosym, Nanobiotix, Noveome, Particles for Humanity, Perosphere, Pfizer, Polaris, Portal, Pulmatrix, Puretech, Roche, Rubius, Secant, Selecta Biosciences, Setsuro, Shiseido, Sigilon, Sio2, SQZ, Stembiosys, Suono Bio, T2 Biosystems, Tara, Taris Biomedical, Tarveda, Third Rock, Tiba, Titan Pharma, Unilever, VasoRX, Verseau Therapeutics, Vivtex, Wiki Foods, and Zenomics. The remaining authors declare no competing interests.

ACKNOWLEDGMENTS

We acknowledge the Swanson Biotechnology Center at the Koch Institute for Integrative Cancer Research for help with histology, the Keck Imaging Center at the Whitehead Institute for help with electron microscopy imaging, and Amanda del Rosario and the MIT proteomics core facility for help with the proteomics analysis. This work was supported by MIT Skoltech grant No.182-MRA, United States; Skoltech internal grant to Victor Koteliansky, Russia; Russian Scientific Fund (14-34-00017), Russia, and NIH grants (DK117149 and GM065204), United States.

REFERENCES

1. Mills, E.W., and Green, R. (2017). Ribosomopathies: there's strength in numbers. Science *358*, eaan2755.
2. Barna, M., Pusic, A., Zollo, O., Costa, M., Kondrashov, N., Rego, E., Rao, P.H., and Ruggero, D. (2008). Suppression of Myc oncogenic activity by ribosomal protein haploinsufficiency. Nature *456*, 971–975.
3. Montanaro, L., Treré, D., and Derenzini, M. (2012). Changes in ribosome biogenesis may induce cancer by down-regulating the cell tumor suppressor potential. Biochim Biophys Acta *1825*, 101–110.
4. Silvera, D., Formenti, S.C., and Schneider, R.J. (2010). Translational control in cancer. Nat. Rev. Cancer *10*, 254–266.
5. Chikashige, Y., Arakawa, S., Leibnitz, K., Tsutsumi, C., Mori, C., Osakada, H., Murata, M., Haraguchi, T., and Hiraoka, Y. (2015). Cellular economy in fission yeast cells continuously cultured with limited nitrogen resources. Sci. Rep. *5*, 15617.
6. Sinturel, F., Gerber, A., Mauvoisin, D., Wang, J., Gatfield, D., Stubblefield, J.J., Green, C.B., Gachon, F., and Schibler, U. (2017). Diurnal oscillations in liver mass and cell size accompany ribosome assembly cycles. Cell *169*, 651–663.e14.
7. Ingolia, N.T. (2016). Ribosome footprint profiling of translation throughout the genome. Cell *165*, 22–33.
8. Sonenberg, N., and Hinnebusch, A.G. (2009). Regulation of translation initiation in eukaryotes: mechanisms and biological targets. Cell *136*, 731–745.
9. Hinnebusch, A.G., Ivanov, I.P., and Sonenberg, N. (2016). Translational control by 5′-untranslated regions of eukaryotic mRNAs. Science *352*, 1413–1416.
10. Truitt, M.L., Conn, C.S., Shi, Z., Pang, X., Tokuyasu, T., Coady, A.M., Seo, Y., Barna, M., and Ruggero, D. (2015). Differential requirements for eIF4E dose in normal development and cancer. Cell *162*, 59–71.
11. Brina, D., Miluzio, A., Ricciardi, S., Clarke, K., Davidsen, P.K., Viero, G., Tebaldi, T., Offenhäuser, N., Rozman, J., Rathkolb, B., et al. (2015). eIF6 coordinates insulin sensitivity and lipid metabolism by coupling translation to transcription. Nat. Commun. *6*, 8261.
12. Cattie, D.J., Richardson, C.E., Reddy, K.C., Ness-Cohn, E.M., Droste, R., Thompson, M.K., Gilbert, W.V., and Kim, D.H. (2016). Mutations in nonessential eIF3k and eIF3l genes confer lifespan extension and enhanced resistance to ER stress in Caenorhabditis elegans. PLoS Genet. *12*, e1006326.
13. Choudhuri, A., Maitra, U., and Evans, T. (2013). Translation initiation factor eIF3h targets specific transcripts to polysomes during embryogenesis. Proc. Natl. Acad. Sci. USA *110*, 9818–9823.
14. Huijbers, I.J. (2017). Generating genetically modified mice: a decision guide. Methods Mol. Biol. *1642*, 1–19.
15. Valášek, L.S., Zeman, J., Wagner, S., Beznosková, P., Pavlíková, Z., Mohammad, M.P., Hronová, V., Herrmannová, A., Hashem, Y., and Gunišová, S. (2017). Embraced by eIF3: structural and functional insights into the roles of eIF3 across the translation cycle. Nucleic Acids Res. *45*, 10948–10968.

16. Lee, A.S.Y., Kranzusch, P.J., and Cate, J.H.D. (2015). eIF3 targets cell-proliferation messenger RNAs for translational activation or repression. Nature *522*, 111–114.

17. Lee, A.S.Y., Kranzusch, P.J., Doudna, J.A., and Cate, J.H.D. (2016). eIF3d is an mRNA cap-binding protein that is required for specialized translation initiation. Nature *536*, 96–99.

18. Shah, M., Su, D., Scheliga, J.S., Pluskal, T., Boronat, S., Motamedchaboki, K., Campos, A.R., Qi, F., Hidalgo, E., Yanagida, M., and Wolf, D.A. (2016). A transcript-specific eIF3 complex mediates global translational control of energy metabolism. Cell Rep. *16*, 1891–1902.

19. Zeng, L., Wan, Y., Li, D., Wu, J., Shao, M., Chen, J., Hui, L., Ji, H., and Zhu, X. (2013). The m subunit of murine translation initiation factor eIF3 maintains the integrity of the eIF3 complex and is required for embryonic development, homeostasis, and organ size control. J. Biol. Chem. *288*, 30087–30093.

20. Wagner, S., Herrmannová, A., Šikrová, D., and Valášek, L.S. (2016). Human eIF3b and eIF3a serve as the nucleation core for the assembly of eIF3 into two interconnected modules: the yeast-like core and the octamer. Nucleic Acids Res. *44*, 10772–10788.

21. Smith, M.D., Arake-Tacca, L., Nitido, A., Montabana, E., Park, A., and Cate, J.H. (2016). Assembly of eIF3 mediated by mutually dependent subunit insertion. Structure *24*, 886–896.

22. Love, K.T., Mahon, K.P., Levins, C.G., Whitehead, K.A., Querbes, W., Dorkin, J.R., Qin, J., Cantley, W., Qin, L.L., Racie, T., et al. (2010). Lipid-like materials for low-dose, *in vivo* gene silencing. Proc. Natl. Acad. Sci. USA *107*, 1864–1869.

23. Bogorad, R.L., Yin, H., Zeigerer, A., Nonaka, H., Ruda, V.M., Zerial, M., Anderson, D.G., and Koteliansky, V. (2014). Nanoparticle-formulated siRNA targeting integrins inhibits hepatocellular carcinoma progression in mice. Nat. Commun. *5*, 3869.

24. Zeigerer, A., Gilleron, J., Bogorad, R.L., Marsico, G., Nonaka, H., Seifert, S., Epstein-Barash, H., Kuchimanchi, S., Peng, C.G., Ruda, V.M., et al. (2012). Rab5 is necessary for the biogenesis of the endolysosomal system *in vivo*. Nature *485*, 465–470.

25. Pei, Y., and Tuschl, T. (2006). On the art of identifying effective and specific siRNAs. Nat. Methods *3*, 670–676.

26. Frank-Kamenetsky, M., Grefhorst, A., Anderson, N.N., Racie, T.S., Bramlage, B., Akinc, A., Butler, D., Charisse, K., Dorkin, R., Fan, Y., et al. (2008). Therapeutic RNAi targeting PCSK9 acutely lowers plasma cholesterol in rodents and LDL cholesterol in nonhuman primates. Proc. Natl. Acad. Sci. USA *105*, 11915–11920.

27. Querbes, W., Bogorad, R.L., Moslehi, J., Wong, J., Chan, A.Y., Bulgakova, E., Kuchimanchi, S., Akinc, A., Fitzgerald, K., Koteliansky, V., and Kaelin, W.G., Jr. (2012). Treatment of erythropoietin deficiency in mice with systemically administered siRNA. Blood *120*, 1916–1922.

28. Napolitano, M., Siragusa, S., and Mariani, G. (2017). Factor VII deficiency: clinical phenotype, genotype and therapy. J. Clin. Med. *6*, E38.

29. Khajuria, R.K., Munschauer, M., Ulirsch, J.C., Fiorini, C., Ludwig, L.S., McFarland, S.K., Abdulhay, N.J., Specht, H., Keshishian, H., Mani, D.R., et al. (2018). Ribosome levels selectively regulate translation and lineage commitment in human hematopoiesis. Cell *173*, 90–103.e19.

30. Brunt, E.M. (2007). Pathology of fatty liver disease. Mod. Pathol. *20* (*Suppl 1*), S40–S48.

31. Wiita, A.P., Ziv, E., Wiita, P.J., Urisman, A., Julien, O., Burlingame, A.L., Weissman, J.S., and Wells, J.A. (2013). Global cellular response to chemotherapy-induced apoptosis. eLife *2*, e01236.

32. Andreev, D.E., O'Connor, P.B., Zhdanov, A.V., Dmitriev, R.I., Shatsky, I.N., Papkovsky, D.B., and Baranov, P.V. (2015). Oxygen and glucose deprivation induces widespread alterations in mRNA translation within 20 minutes. Genome Biol. *16*, 90.

33. Pulos-Holmes, M.C., Srole, D.N., Juarez, M.G., Lee, A.S., McSwiggen, D.T., Ingolia, N.T., and Cate, J.H. (2019). Repression of ferritin light chain translation by human eIF3. eLife *8*, e48193.

34. Subramanian, A., Tamayo, P., Mootha, V.K., Mukherjee, S., Ebert, B.L., Gillette, M.A., Paulovich, A., Pomeroy, S.L., Golub, T.R., Lander, E.S., and Mesirov, J.P. (2005). Gene set enrichment analysis: a knowledge-based approach for interpreting genome-wide expression profiles. Proc. Natl. Acad. Sci. USA *102*, 15545–15550.

35. Kanehisa, M., and Goto, S. (2000). KEGG: Kyoto encyclopedia of genes and genomes. Nucleic Acids Res. *28*, 27–30.

36. Hu, H., and Li, X. (2007). Transcriptional regulation in eukaryotic ribosomal protein genes. Genomics *90*, 421–423.

37. Calo, E., Flynn, R.A., Martin, L., Spitale, R.C., Chang, H.Y., and Wysocka, J. (2015). RNA helicase DDX21 coordinates transcription and ribosomal RNA processing. Nature *518*, 249–253.

38. Joo, Y.J., Kim, J.-H., Kang, U.-B., Yu, M.-H., and Kim, J. (2011). Gcn4p-mediated transcriptional repression of ribosomal protein genes under amino-acid starvation. EMBO J. *30*, 859–872.

39. Munchel, S.E., Shultzaberger, R.K., Takizawa, N., and Weis, K. (2011). Dynamic profiling of mRNA turnover reveals gene-specific and system-wide regulation of mRNA decay. Mol. Biol. Cell *22*, 2787–2795.

40. Borowski, L.S., and Szczesny, R.J. (2014). Measurement of mitochondrial RNA stability by metabolic labeling of transcripts with 4-thiouridine. Methods Mol. Biol. *1125*, 277–286.

41. Kim, S., Li, Q., Dang, C.V., and Lee, L.A. (2000). Induction of ribosomal genes and hepatocyte hypertrophy by adenovirus-mediated expression of c-Myc *in vivo*. Proc. Natl. Acad. Sci. USA *97*, 11198–11202.

42. Chaillou, T., Kirby, T.J., and McCarthy, J.J. (2014). Ribosome biogenesis: emerging evidence for a central role in the regulation of skeletal muscle mass. J. Cell. Physiol. *229*, 1584–1594.

43. van Riggelen, J., Yetil, A., and Felsher, D.W. (2010). MYC as a regulator of ribosome biogenesis and protein synthesis. Nat. Rev. Cancer *10*, 301–309.

44. Mandal, A., Mandal, S., and Park, M.H. (2016). Global quantitative proteomics reveal up-regulation of endoplasmic reticulum stress response proteins upon depletion of eIF5A in HeLa cells. Sci. Rep. *6*, 25795.

45. Mi, H., Muruganujan, A., and Thomas, P.D. (2013). PANTHER in 2013: modeling the evolution of gene function, and other gene attributes, in the context of phylogenetic trees. Nucleic Acids Res. *41* (Database issue, D1), D377–D386.

46. Pakos-Zebrucka, K., Koryga, I., Mnich, K., Ljujic, M., Samali, A., and Gorman, A.M. (2016). The integrated stress response. EMBO Rep. *17*, 1374–1395.

47. Kaul, G., Pattan, G., and Rafeequi, T. (2011). Eukaryotic elongation factor-2 (eEF2): its regulation and peptide chain elongation. Cell Biochem. Funct. *29*, 227–234.

48. Mullineux, S.-T., and Lafontaine, D.L.J. (2012). Mapping the cleavage sites on mammalian pre-rRNAs: where do we stand? Biochimie *94*, 1521–1532.

49. Bruno, P.M., Liu, Y., Park, G.Y., Murai, J., Koch, C.E., Eisen, T.J., Pritchard, J.R., Pommier, Y., Lippard, S.J., and Hemann, M.T. (2017). A subset of platinum-containing chemotherapeutic agents kills cells by inducing ribosome biogenesis stress. Nat. Med. *23*, 461–471.

50. Dong, Y., Love, K.T., Dorkin, J.R., Sirirungruang, S., Zhang, Y., Chen, D., Bogorad, R.L., Yin, H., Chen, Y., Vegas, A.J., et al. (2014). Lipopeptide nanoparticles for potent and selective siRNA delivery in rodents and nonhuman primates. Proc. Natl. Acad. Sci. USA *111*, 3955–3960.

51. Yin, H., Bogorad, R.L., Barnes, C., Walsh, S., Zhuang, I., Nonaka, H., Ruda, V., Kuchimanchi, S., Nechev, L., Akinc, A., et al. (2016). RNAi-nanoparticulate manipulation of gene expression as a new functional genomics tool in the liver. J. Hepatol. *64*, 899–907.

52. McGowan, K.A., and Mason, P.J. (2011). Animal models of Diamond Blackfan anemia. Semin. Hematol. *48*, 106–116.

53. Tschochner, H., and Hurt, E. (2003). Pre-ribosomes on the road from the nucleolus to the cytoplasm. Trends Cell Biol. *13*, 255–263.

54. Adams, D., Suhr, O.B., Dyck, P.J., Litchy, W.J., Leahy, R.G., Chen, J., Gollob, J., and Coelho, T. (2017). Trial design and rationale for APOLLO, a phase 3, placebo-controlled study of patisiran in patients with hereditary ATTR amyloidosis with polyneuropathy. BMC Neurol. *17*, 181.

55. Corsini, N.S., Peer, A.M., Moeseneder, P., Roiuk, M., Burkard, T.R., Theussl, H.-C., Moll, I., and Knoblich, J.A. (2018). Coordinated control of mRNA and rRNA processing controls embryonic stem cell pluripotency and differentiation. Cell Stem Cell *22*, 543–558.e12.

56. Radhakrishnan, A., Chen, Y.-H., Martin, S., Alhusaini, N., Green, R., and Coller, J. (2016). The DEAD-box protein Dhh1p couples mRNA decay and translation by monitoring codon optimality. Cell *167*, 122–132.e9.

57. Presnyak, V., Alhusaini, N., Chen, Y.-H., Martin, S., Morris, N., Kline, N., Olson, S., Weinberg, D., Baker, K.E., Graveley, B.R., and Coller, J. (2015). Codon optimality is a major determinant of mRNA stability. Cell *160*, 1111–1124.

58. Sammarco, M.C., Ditch, S., Banerjee, A., and Grabczyk, E. (2008). Ferritin L and H subunits are differentially regulated on a post-transcriptional level. J. Biol. Chem. *283*, 4578–4587.

59. Kos-Braun, I.C., Jung, I., and Koš, M. (2017). Tor1 and CK2 kinases control a switch between alternative ribosome biogenesis pathways in a growth-dependent manner. PLoS Biol. *15*, e2000245.

60. Tanaka, Y., Okamoto, K., Teye, K., Umata, T., Yamagiwa, N., Suto, Y., Zhang, Y., and Tsuneoka, M. (2010). JmjC enzyme KDM2A is a regulator of rRNA transcription in response to starvation. EMBO J. *29*, 1510–1522.

61. Anand, P., and Gruppuso, P.A. (2005). The regulation of hepatic protein synthesis during fasting in the rat. J. Biol. Chem. *280*, 16427–16436.

62. Fonseca, B.D., Smith, E.M., Yelle, N., Alain, T., Bushell, M., and Pause, A. (2014). The ever-evolving role of mTOR in translation. Semin. Cell Dev. Biol. *36*, 102–112.

63. Watanabe-Asano, T., Kuma, A., and Mizushima, N. (2014). Cycloheximide inhibits starvation-induced autophagy through mTORC1 activation. Biochem. Biophys. Res. Commun. *445*, 334–339.

64. Ban, N., Beckmann, R., Cate, J.H., Dinman, J.D., Dragon, F., Ellis, S.R., Lafontaine, D.L.J., Lindahl, L., Liljas, A., Lipton, J.M., et al. (2014). A new system for naming ribosomal proteins. Curr. Opin. Struct. Biol. *24*, 165–169.